Evaluating the Economic Potential of Part of Ife-Ilesha Schist Belt, Western Nigeria, Using Airborne Magnetic and Radiometric Dataset

[1] Nwokeabia Nkiru, [2]Uche Iduma, [3] Ibe Stephen O.

[1]Nnamdi Azikwe University Awka Nigeria,
[2]Nigerian Geological Survey Agency, [3]Federal University Otuoke Bayelsa Nigeria.
Corresponding Author: Ibe Stephen O.

Abstract: *Evaluation of the part of Ife-Ilesha Schist Belt was done to define the structures, geology and map out alteration zones related to ore deposits. Datasets from airborne geophysical method proved vital for mapping geology and structures within Ondo extension of the Ife-Ilesha Schist Belt. The total magnetic intensity data covering the basement complex was processed and filtered using Reduce to Pole, Analytic Signal (ANSIG) and First vertical derivative (FVD) filters. Trend analysis was applied to the data to produce the residual field component of the data after which the FVD was computed to enhance folds, fractures and lithological contact. The main structural or early deformation event emplaced NNE-SSW structures and the second deformation event emplaced and reoriented the main structures to NE-SW and these are potential hydrothermal gold mineralization zones within the area. The faults and contacts between schist metasediments and metavolcanic rocks noted to host gold mineralization in the Ife-Ilesha Belt were also delineated. The radiometric datasets retrieving geochemical information on potassium (K), thorium (Th) and uranium (U) concentrations within the study area were used to delineate bedrock lithology of the Granite, schist, gneiss, as well as alteration and contact zones. The high resolution airborne magnetic and radiometric data of the study area resulted in better definition of both geological structures and lithological boundaries. This research shows the economic potential of the Ife-Ilesha Schist Belt within Ondo area, as this has not been previously evaluated by any author.*
Keywords*: Ondo, Ife, Ilesha, Ifewara, Odigbo, aeromagnetic, tilt derivative, analytic signal, radiometric, hydrothermal, alteration, mineral exploration, meneralization*

I. Introduction

Overlying the Archaean gneissic complex in Nigeria are widespread Proterozoic metasediments, which include variable volcanic components, well developed as elongated N-S trending belts in the western half of Nigeria. There are no affirmative ages of formation for metasediments in Nigeria and the Borborema province of NE Brazil. Inferred depositional ages for the Palaeoproterozoic series in these areas straddle from 2.2 to 2.0 Ga and predate the 1.9–1.8 Ga igneous activities (Grant, 1970; Rahaman and Emofurieta, 1983; Rahaman and Lancelot, 1984; Jardim de Sa *et al.,* 1987; Annor, 1995; Neves *et al.,* 2006). In addition to the well-developed medium to high grade schists, the Neoproterozoic series of mainly low grade, weakly deformed metasediments occur in association with the thermal aureole of Pan-African granitoids and show upper greenschist to low pressure amphibolite facies metamorphism. More recent work on the same series in NE Brazil (Van Schmus *et al.,* 2003; Neves *et al.,* 2009), their structural relationships with Pan-African granitoids as well as their unequivocal reworking suggest a Neoproterozoic age of deposition. Gold and other metallic deposits occur in these rocks in Brazil and Nigeria and the Pan African is widely accepted as the minimum age of gold and associated mineralization in this belt. Neoproterozoic granitoids in Nigeria consist of several contemporaneous petrologic groups. Their formation ages are well constrained between 640 and 580 Ma (Tubosun *et al.*, 1984; Dada and Respaut, 1989; Dada *et al.*, 1989; Rahaman *et al.*, 1991). The well-defined Pan-African deformation pattern in the Nigerian schist belts has been related to gold and associated mineralization.

The Ife - Ilesha Schist Belt is characterized by meta-sediments and metavolcanic, migmatite gneiss and older granite rocks and the occurance of a shear zone that has been traced to and correlated with the central Hoggar Neoproteozoic shear zone as part of the Trans-Saharan Belt (Rahaman, 1976). The reactivation of the structures has had a profound effect in the mode of occurrences and distribution of gold deposit in the country (Olusegun, *et al.*, 1995). Structures in the area are certainly complex and feature tightly folded and faulted schist, granite and gneiss (Hubbard, 1960., Rahaman, 1976); the trends of the major faults as well as the fold planes, strike to the NE and dip steeply to the NW. The major fault system is part of the Ife-Ilesha fault system defined that stretches for more than 100km and classified to be highly mineralized (Rahaman, 1976; Kayode, 2006), occurring within the schist belt of southwestern Nigeria.

Airborne surveys such as aeromagnetic and radiometric data, provides fast coverage of large and inaccessible areas for subsurface reconnaissance, which makes magnetic data analysis an essential tool of geophysical exploration. This past decade has witnessed a paradigm shift from the interpretation of basement structures to detailed studies with respect to both lithologic and morphologic variations. Its application ranges from mineral exploration (Murphy, 2007), structure mapping and rock characterization (Telford *et al*., 1990). Recent advances in technology have substantially increased the accuracy and resolution of these techniques so that they can be used to provide useful enhanced information on lithology and geological structures. Additionally, advances in data analysis, processing and image enhancement techniques have improved the resolution of geophysical datasets further so that very subtle variations in the geophysical responses can be identified (Armstrong and Rodeghiero, 2006).

Magnetic anomalies are major precursor of mineralization, especially along fault planes. The magnetic anomaly signature characteristics are results of one or more physical parameters such as the configuration of the anomalous zone, magnetic susceptibility contrasts as well as the depth to the anomalous body. Wilford *et al*. (1997) indicated that airborne radiometric survey similarly is used to measure variations in the radioactive mineral composition in order to map lateral lithological changes. This method involves the measurement of naturally occurring radioactive elements that exist in rock forming minerals and soil profiles. These elements are uranium (U), thorium (Th) and potassium (K), which can be found as trace elements in all rocks and decay naturally giving off gamma radiation (gamma rays). The variation of magnetic and radiometric mineral composition in rocks due to the distinction in lithological set up and mineralization processes such as hydrothermal mineralization make the use of these methods in the mapping rock lithology, structures and mineral zones an important technique.

This paper discusses aeromagnetic and radiometric datasets from Ondo area of the Ife-Ife-Ilesha Schist Belt of Nigeria. Airborne magnetic and radiometric data were used to map the geology and delineated possible gold hosting structure within this part of the belt. This part of the belt has never been evaluated or studied using this method, hence the importance of the study. This research seeks to review the geology and to aid the delineation of regional and local geological structures (shear zones and faults) that have the potential of hosting gold mineralization within the study area. The work allows the prediction of target areas for detailed exploration work in search for metal ore mineralization within the Ondo area that has not been extensively explored as compared to the other parts of the Ife-Ilesha Belt.

II. Materials and Method
2.1 The Study Area
The area is bounded by longitudes $4^o22'\ 00''E$ to $4^o47'\ 00''E$ and latitudes $6^o45'\ 00'N$ to $7^o27''\ 00'N$. The study area covers approximately 3,025km^2; including Ondo, Iperindo, Ife, Wanikin, Olomu, Ashewele and Odigbo. The area can be accessed through Akure-Ondo expressway, Ife-Ondo expressway and Ore-Ondo expressway. It falls within the humid tropical region with two distinct seasons, the rainy season, from March to October, and dry season, from November to March. The annual rainfall in the area is estimated to be about 2,000 mm (Ondo State Ministry of Economic Planning & Budget, 2010) with mean monthly temperature range of 25.7°C to 30.2°C and high humidity, generally above 50% (Ondo State Ministry of Lands, Housing & Environment, 2000). Ondo township falls within the Pre-Cambrian Basement Complex of Southwestern Nigeria which consists of migmatite, gneisses, schist and quartzite into which has been an emplacement of granitic and, to a lesser extent, more basic materials (Rahaman, 1981). The dominant rock types in the area are the medium to coarse grained granite, granite gneiss and quartzite (Figure 1).
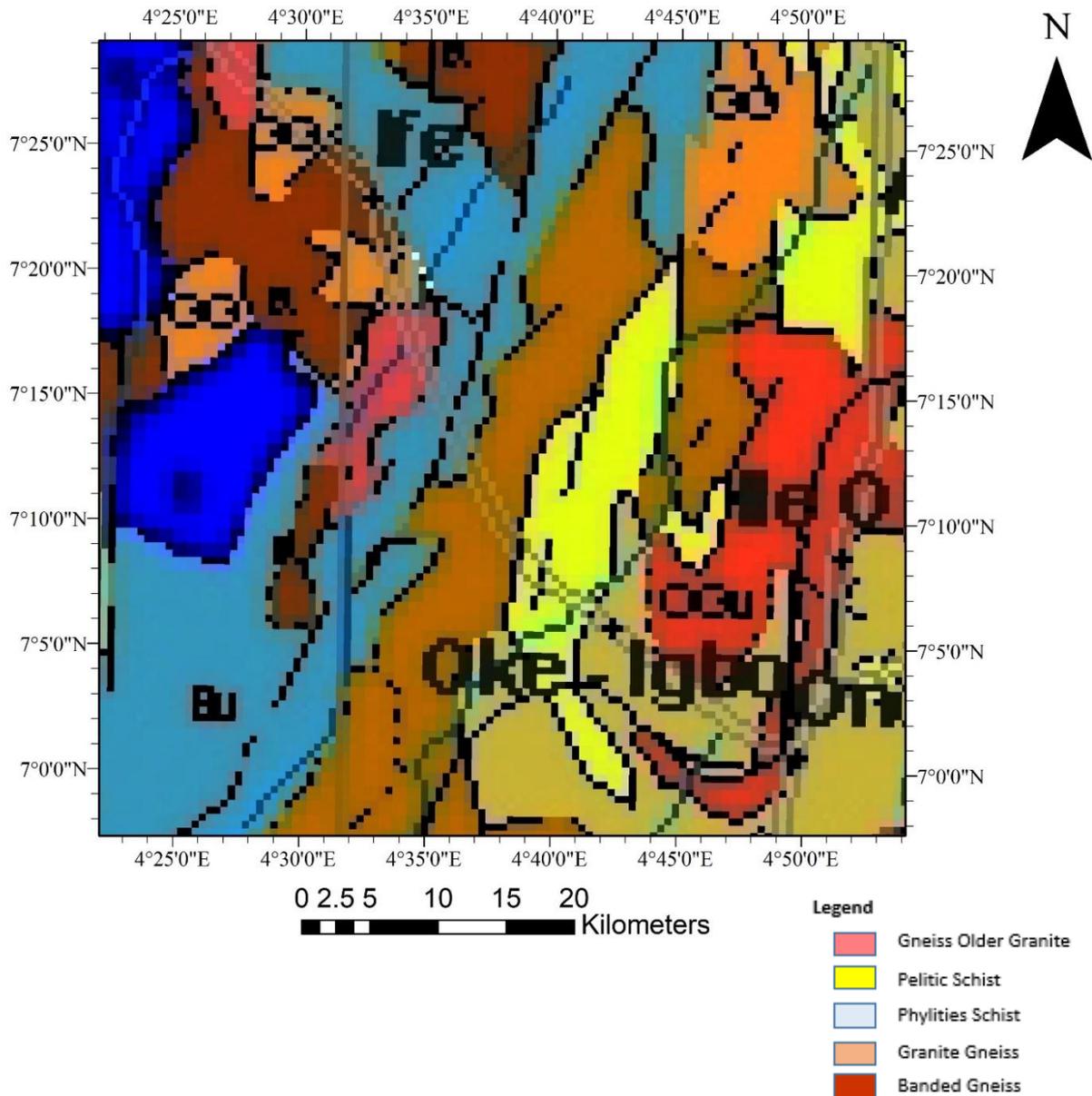
Figure 1: Geology of the Study Area

2.2   Data Acquisition

The aeromagnetic dataset used for this study is from the high-resolution airborne survey coverage in Nigeria carried out by Fugro Airborne Survey at 826,000 along a series of NW – SE flight lines of magnetic and radiometric surveys flown at 500 m line spacing and 80m terrain clearance in 2009 and was obtained from the Nigerian Geological Survey Agency. The parameter measured was the total magnetic field. It consists of one square blocks of map sheet (263) of square block which represents a map on the scale of 1:100,000 and is (55×55) km^2 covering an area of 3,025km². The total magnetic intensity grid was generated using a minimum curvature algorithm at a grid cell size of 1,000 m. The digitized data were filtered using a low pass Fourier domain sub-routine filter to eliminate unwanted wavelengths and to pass longer wavelengths. Reduction-to-pole (RTP) transformation was applied to the aeromagnetic data to minimize polarity effects. These effects are manifested as a shift of the main anomaly from the center of the magnetic source and are due to the vector nature of the measured magnetic field. The RTP transformation usually involves an assumption that the total magnetizations of most rocks align parallel or anti-parallel to the Earth's main field.

2.3 Data Processing and Enhancement
2.3.1 Regional - residual separation

Separation of regional and residual anomaly was done using Trend analysis in which a linear trend surface was fitted into the total aeromagnetic field data by a multiple regression technique for the purpose of removing the regional magnetic field. The linear surface fitted was removed from the regional component to obtain the residual magnetic anomaly map that was interpreted.

$$Total\ field = Regional\ field + Residual\ field \tag{1}$$
$$Residual\ field = Total\ field - fitted\ Surface/Regional \tag{2}$$

The Regional Field can be represented using the trend surface equation. Davies, (1973) expressed the regional field as;

$$Regional\ Field = a + bx_i + cy_j \tag{3}$$

Where, a, b and c are constants, x_i and y_j are coordinates in x and y directions.

Let Z_{ij} = the observed Total Field at ij^{th} data point.

Therefore,

$$Total\ Field\ (Z_{ij}) = (a + bx_i + cy_j) + Residual\ Field \tag{4}$$

Hence,

$$Residual\ Field = Z_{ij} - (a + bx_i + cy_j) \tag{5}$$

For a given magnetic data, the best fitting surface has the least square error,

$$fitting\ error = t - a - bx - cy \tag{6}$$

Where t is the magnetic value at x and y coordinate point.

Note that a, b and c are unknown coefficients while t, x and y are given. To obtain the least square error, the unknown coefficients a, b and c must yield zero first partial derivative.

Hence, the sum of the square of the fitting error becomes;

$$\sum_{i=1}^{N}\sum_{j=1}^{N}(fitting\ error)^2 = \sum_{i=1}^{N}\sum_{j=1}^{N}(t_{ij} - a - bx_i - cy_j)^2 \tag{7}$$

where x_i, y_j and t_{ij} are vecctors and i and j are unit vector while t, x and y are coefficients of the unit vector.

$$M = \sum_{i=1}^{N}\sum_{j=1}^{N}(t_{ij} - a - bx_i - cy_j)^2 \tag{8}$$

Taking the partial derivative of equation (8) with respect to a and equate it to zero,

$$\sum_{i=1}^{N}\sum_{j=1}^{N}t_{ij} - \sum_{i=1}^{N}\sum_{j=1}^{N}a - b\sum_{i=1}^{N}\sum_{j=1}^{N}x_i - c\sum_{i=1}^{N}\sum_{j=1}^{N}y_j = 0 \tag{9}$$

Partial derivative of the second constant b and equating it to zero;

$$\sum_{i=1}^{N}\sum_{j=1}^{N}t_{ij}\,x_i - a\sum_{i=1}^{N}\sum_{j=1}^{N}x_i - b\sum_{i=1}^{N}\sum_{j=1}^{N}x_i^2 - c\sum_{i=1}^{N}\sum_{j=1}^{N}x_iy_j = 0 \tag{10}$$

Taking the partial derivative of the third constant c;

$$\sum_{i=1}^{N}\sum_{j=1}^{N}t_{ij}\,y_j - a\sum_{i=1}^{N}\sum_{j=1}^{N}y_j - b\sum_{i=1}^{N}\sum_{j=1}^{N}x_iy_j - c\sum_{i=1}^{N}\sum_{j=1}^{N}y_j^2 = 0 \tag{11}$$

Solving this series of simultaneous equations will give the coefficients of the best fitting linear trend surface, being defined by the least-square criterion. The above equation can be written into matrix form as:

$$\begin{bmatrix} N & \sum_{i=1}^{N}\sum_{j=1}^{N}x_i & \sum_{i=1}^{N}\sum_{j=1}^{N}y_j \\ \sum_{i=1}^{N}\sum_{j=1}^{N}x_i & \sum_{i=1}^{N}\sum_{j=1}^{N}x_i^2 & \sum_{i=1}^{N}\sum_{j=1}^{N}x_iy_j \\ \sum_{i=1}^{N}\sum_{j=1}^{N}y_j & \sum_{i=1}^{N}\sum_{j=1}^{N}x_iy_j & \sum_{i=1}^{N}\sum_{j=1}^{N}y_i^2 \end{bmatrix} \begin{bmatrix} a \\ b \\ c \end{bmatrix} = \begin{bmatrix} \sum_{i=1}^{N}\sum_{j=1}^{N}t_{ij} \\ \sum_{i=1}^{N}\sum_{j=1}^{N}t_{ij}x_i \\ \sum_{i=1}^{N}\sum_{j=1}^{N}t_{ij}y_j \end{bmatrix} \tag{12}$$

The values of a, b, and c were obtained as follows;

$$\left.\begin{array}{lcl} a & = & 7830 \\ b & = & 3.5429 \\ c & = & -3.6132 \end{array}\right\} \tag{13}$$

The trend surface equation (regional gradient) becomes:

$$T(x,y) = 7830 + 3.5429x - 3.6132\,y \tag{14}$$

Furthermore, the trend surface equation was then subtracted from the aeromagnetic (observed) data and the resultant residual anomaly was digitized.

2.3.2 Analytic signal filter

Nabighian (1972) suggested the concept of analytic signal (AS) and proposed that in the 2-D case, the horizontal and vertical derivatives of magnetic fields satisfy the Hilbert transform, thus can be regarded as analytic signals. The amplitude of the analytic signal is the same as the total gradient, independent of the direction of magnetization, and represents the envelope of both the vertical and horizontal derivatives over all possible directions of the earth's field and source magnetization (Luo *et al.*, 2011).

$$\frac{\partial T}{\partial z} = H\left[\frac{\partial T}{\partial x}\right] \tag{15}$$

Where;

T = Magnetic anomaly data

H = Hilbert transform

The analytical signal of a real signal f is defined as;

$$AS\left(\frac{\partial T}{\partial x}\right) = \frac{\partial T}{\partial x} - iH\left[\frac{\partial T}{\partial x}\right] \tag{16}$$

Where:

$i = -1$ (Luo *et al.*, 2011)

According to the definition, the analytical signal of the potential field obtained by combining this two quantities into a two-dimensional quantity known as the analytic signal is given as;

$$AS(x, z) = \frac{\partial T}{\partial x} + i\frac{\partial T}{\partial z} \tag{17}$$

Where:

$\frac{\partial T}{\partial x}$ and $\frac{\partial T}{\partial z}$ = Horizontal and vertical component of the total field respectively,

$T(x, z)$ = Magnitude of the total magnetic field

z and x = Cartesian coordinates for the vertical direction and the direction perpendicular to strike respectively

The amplitude of the analytic signal is defined as;

$$|AS(z)| = \sqrt{\left(\frac{\partial T}{\partial x}\right)^2 + \left(\frac{\partial T}{\partial z}\right)^2} \tag{18}$$

The amplitude of the analytic signal is a symmetric bell-shaped function. By examining its profile across a magnetic source, the analytic signal can be used in interpretation to provide an indication of the edges of the causative body. Similarly for the three dimensional case, the analytic signal is given by;

$$AS(x, y) = \left(\frac{\partial T}{\partial x}\right) + \left(\frac{\partial T}{\partial y}\right) + \left(i\frac{\partial T}{\partial z}\right) \tag{19}$$

Where its amplitude is defined as;

$$|AS(x, y)| = \sqrt{\left(\frac{\partial T}{\partial x}\right)^2 + \left(\frac{\partial T}{\partial y}\right)^2 \left(\frac{\partial T}{\partial z}\right)^2} \tag{20}$$

The maximum value of the analytic signal determines the edges of a magnetic body.

2.3.3 Tilt Angle filter

The tilt angle derivative was first proposed by Miller and Singh (1994) as a tool for locating magnetic sources on magnetic profile data. Tilt angel derivative is the ratio of the vertical derivative to the absolute amplitude of the total horizontal derivative (Ansari and Alamdar 2011). Figure 2 is a schematic diagram used to illustrate the tilt angle filter. Geometrically tilt angle is given as:
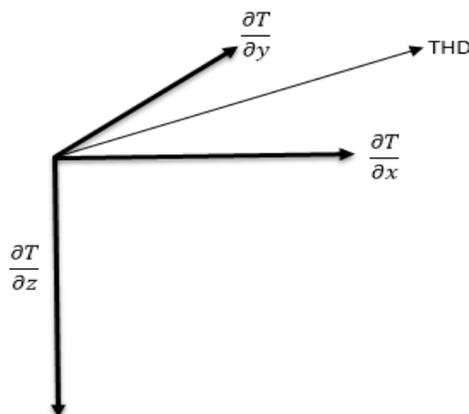

Figure 2: Schematic Diagram to Illustrate the Tilt Angle Filter

$$TAD = \tan^{-2}\left[\frac{VD}{THD}\right] \tag{21}$$

Where:

TAD = Tilt Angle Derivative,

VD = First vertical derivative,
THD = Total horizontal derivative all of the TMI
While VD can be positive or negative, THD is always positive. For grids THD is given as:

$$THD = \sqrt{\left(\frac{\partial T}{\partial x}\right)^2 + \left(\frac{\partial T}{\partial y}\right)^2} \qquad (22)$$

Due to the nature of the arctan trigonometric function, all amplitudes are restricted to values between $+\pi/2$ and $-\pi/2$ $(+90°$ and $-90°)$ regardless of the amplitudes of VD or THD. This fact makes this relationship function like an automatic gain control (AGC) filter and tends to equalize the amplitude output of TMI anomalies across a grid or along a profile (Verduzco *et al.,* 2004).
The tilt angle derivative is therefore given as

$$TAD = tan^{-2}\left[\frac{\frac{\partial T}{\partial z}}{\sqrt{\left(\frac{\partial T}{\partial x}\right)^2 + \left(\frac{\partial T}{\partial y}\right)^2}}\right] \qquad (23)$$

The tilt angle is positive over the source and passes through zero when over or near the edge (Ansari and Alamdar, 2011).

2.3.4   First Vertical derivative

Derivatives (vertical) are based on the principle that the rates of change of magnetic field are sensitive to rock susceptibilities near the ground surface than at depth. First vertical derivative is physically equivalent to measuring the magnetic field simultaneously at two points vertically above each other, subtracting the data and dividing the result by the vertical spatial separation of the measurement points. The first vertical derivative was obtained from Laplace equation which is used to describe the magnetic potential field (U) thus,

$$\frac{\partial^2 U}{\partial x^2} + \frac{\partial^2 U}{\partial y^2} + \frac{\partial^2 U}{\partial z^2} = 0 \qquad (24)$$

but, $-grad \cup = T$ \qquad (25)

Hence,

$$-\frac{\partial T}{\partial x} - \frac{\partial T}{\partial y} - \frac{\partial T}{\partial z} = 0 \qquad (26)$$

Therefore,

$$\frac{\partial T}{\partial z} = -\left(\frac{\partial T}{\partial x} + \frac{\partial T}{\partial y}\right) \qquad (27)$$

Where, $\cup = magnetic\ potential\ field$
$T = total\ magnetic\ field\ vector$
Rewriting equation (27) in numerical form we have,

$$-\frac{\partial T}{\partial x} = \left[\frac{T(x+\Delta x) - T(x)}{\Delta x} + 0(\Delta x)\right] \qquad (28)$$

$0(\Delta x) = error\ terms$ \qquad (29)

$$-\frac{\partial T}{\partial x} = \left[\frac{T(x+\Delta x) - T(x)}{\Delta x}\right] \qquad (30)$$

Similarly,

$$-\frac{\partial T}{\partial y} = \left[\frac{T(y+\Delta y) - T(y)}{\Delta y}\right] \qquad (31)$$

Therefore,

$$\frac{\partial T}{\partial z} = -\left[\frac{T(x+\Delta x) - T(x)}{\Delta x}\right] - \left[\frac{T(y+\Delta y) - T(y)}{\Delta y}\right] \qquad (32)$$

Equation (32) was applied on TMI grid to produce the first derivative map.
$$\Delta x = grid\ interval\ in\ x - direction$$
$$\Delta y = grid\ interval\ in\ y - direction$$

III. Result and Discussion

Airborne magnetic and radiometric datasets were used to delineate the geology, structure and alteration zones in the study area. The airborne magnetic method is based on the measurement of the ambient magnetic susceptibility of geologic bodies and the use of the acquired data to determine the distribution of magnetic minerals (changes in lithology). Radiometric method in exploration is a measure of variations in the radio-elemental mineral (potassium, thorium and uranium) composition and is directly used to map out lateral lithological changes. Integration of the data from these survey methods was used extensively for the delineation of geologic structures and metalliferous deposits within the study area.

3.1   Interpretation of the Magnetic Data

The Shuttle Radar Topography Mission (SRTM) model (Figure 3) reflected the elevation distribution of the study area with the highlands ranging from 200 m – 400 m and located at the north (H1), north-eastern (H2), east (H3) and south-eastern (H4) parts of the area, separated by thin low elevated regions. A moderately elevated region ranging from 170 m to 200 m lies at the central (M1) and in the western (M2) parts of the area stretching north-western (M3) direction, while a very low elevated region with range below 170m (L1, L2 and L3) is observed at the southern, south-western and western parts of the area which is likely to accumulate weathered debris from the high elevated area.

The residual magnetic intensity (RMI) map (Figure 4) emphasizes the intensity and the wavelengths of local anomalies. The rock formations at low magnetic latitude are magnetized parallel to the Earth's magnetic field: hence most of the magnetic anomalies correlate weakly with the expected magnetic signatures of the meta-sediments and metavolcanic in the area. Therefore expected high and low magnetic anomalies of the mafic and felsic rocks are represented by low and high anomalies respectively. The very low magnetic regions lie within high elevated regions (H1, H2, H3 and H4) and is interpreted to be metavolcanic (MV) rocks while the high magnetic anomaly associated with low (G1 and G5) and moderate (G2, G3, G4, G6, G7, G8 and G9) elevation corresponds to granitoid (expected to produce a low to moderate magnetic signature due to mainly low magnetite mineral content). The metasediments MS2, MS3, MS4 and MS5 (Figure 4) at the moderate to low H2, H3 and M1 elevations (Figure 3) registered low to moderate magnetic anomaly due to the low concentration of iron forming minerals while the metasediment, MS1 at the lowland (L3) recorded high magnetic response due to weathering and accumulation of iron rich minerals from the highland.
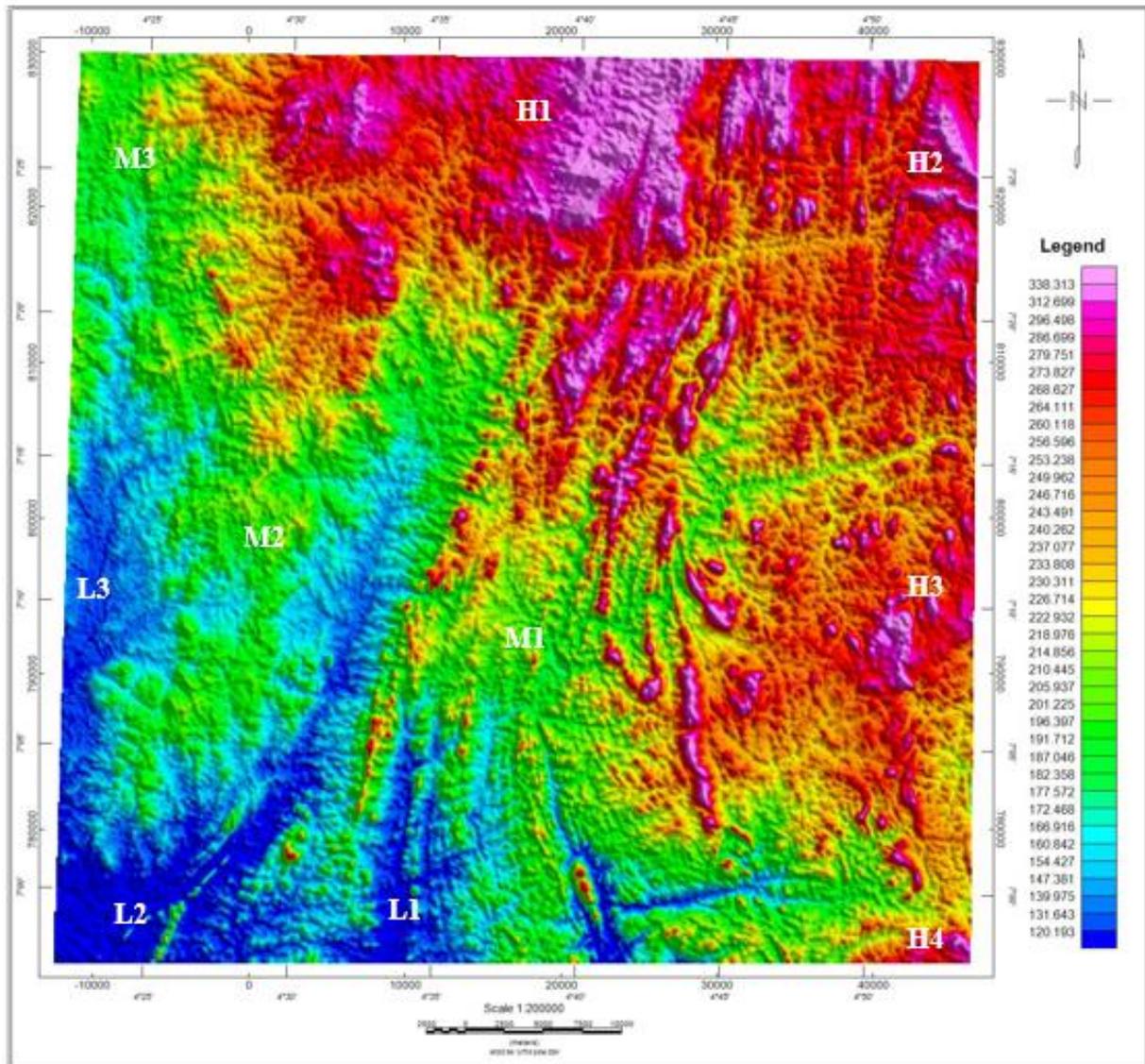

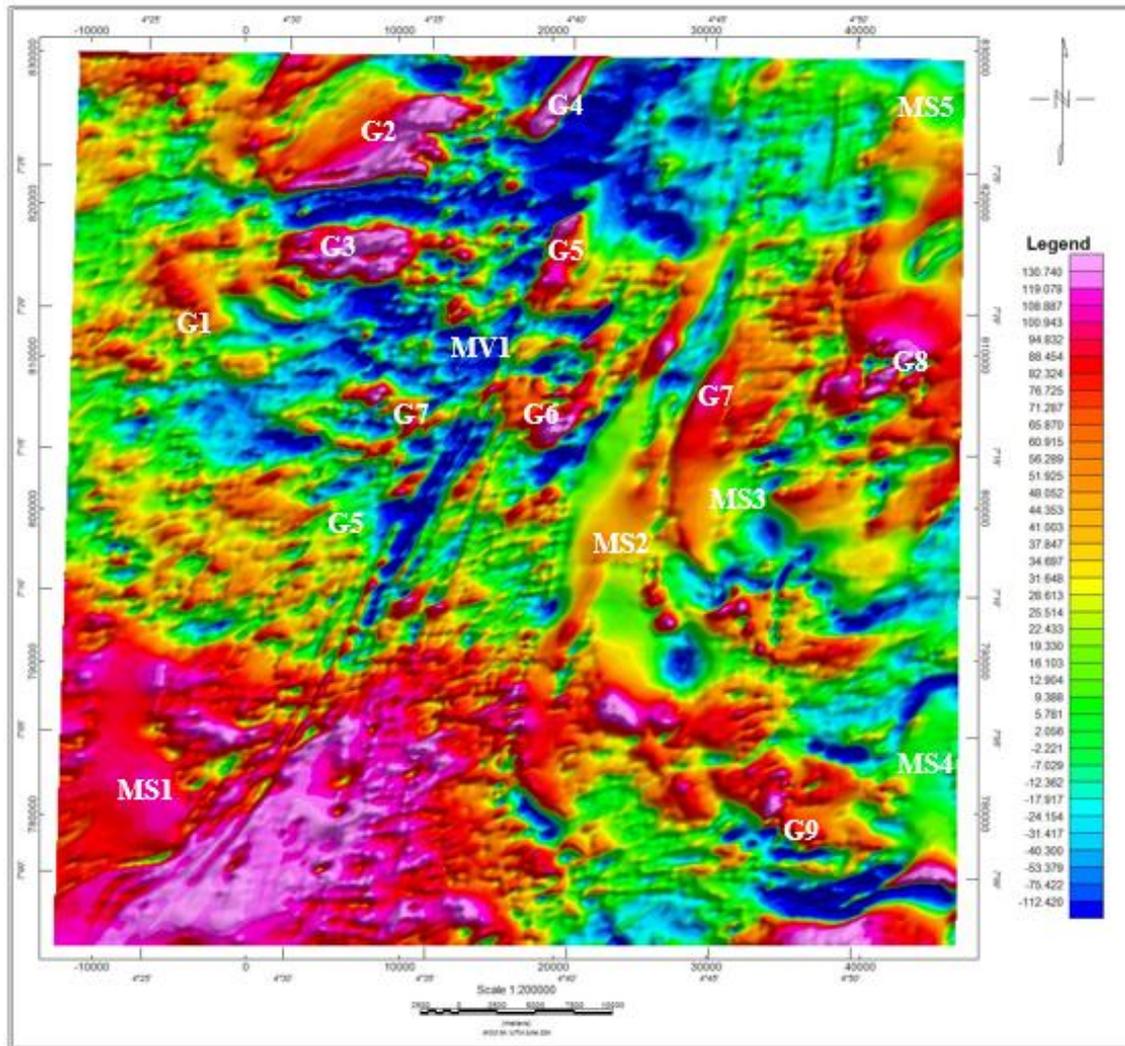**Figure 3:** *Shuttle Radar Topography Mission (SRTM) Model*

Figure 4: Residual Magnetic Intensity (RMI) Map of the Study Area

To identify the observed magnetic anomalies directly over the magnetic source bodies, the TMI grid was transformed into reduction to the pole (RTP) grid map (Murphy, 2007) using the 2D-FFT filter. This map of RTP (Figure 5) sharpens the contacts between the magnetic high and low patterns as well as anomalously high magnetic susceptible zones. The dataset tends to show similar anomaly when the data were reduced to the pole.
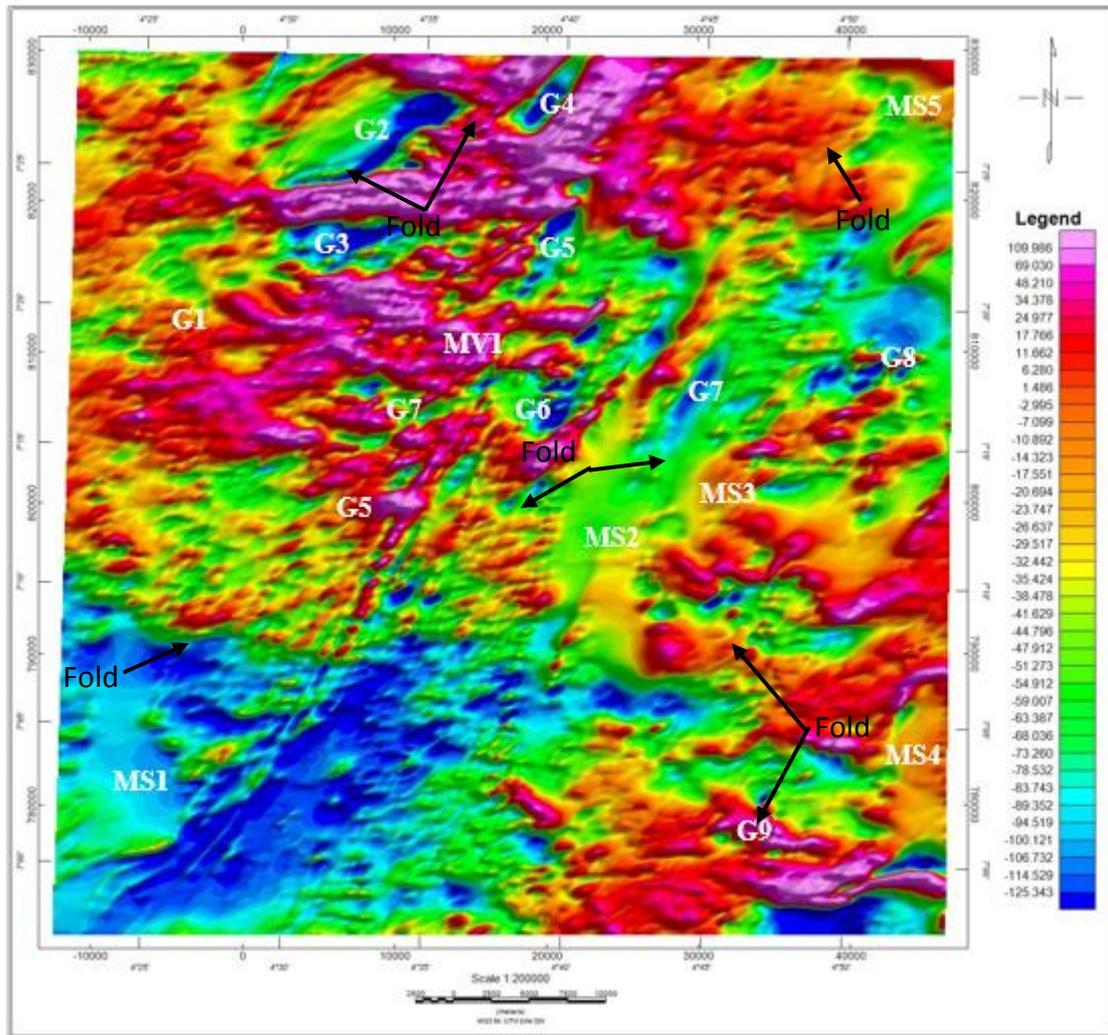
Figure 5: Reduce to Pole Map of the Study Area

The granitoid with high magnetic signature (low in RTP), G2, G3, G4, G5, G6 and G7 was interpreted to have intruded the metavolcanic MV at the northern and central parts of the area (Figure 5). A change in the magnetic amplitude of the granitoids from low to high when reduced to the pole would indicate that they are felsic belt-type granitoids that intruded the area. The contact zones of the belt-type granitoids (G1), metavolcanics (MV1) and metasediments (MS1, MS2, MS3 and MS4) reflect low magnetic anomaly which indicates demagnetization of magnetite minerals to hematite minerals with low magnetic response as a result of hydrothermal fluid flow through the fractures and faults. This is as a result of severe shearing and faulting within these formations.

The features shown in the reduction to the pole inverted map better defined the mafic metavolcanics (MV1) at the northern part of the area. The folding (Fold in Figure 5) at the boundary of the metasedimets-metavolcanics contact is better defined, hence indicating that the influence of magnetic data on the angle of magnetic inclination has been subtracted. After applying the RTP filter to the TMI, the parent formations in Figure 5 reflect the expected magnetic anomalies which translate into the amount of magnetite present in the rocks, with mafic rocks (MV) showing high magnetic signature and felsic rocks (granitoids) showing lower signatures.

The Analytic signal filter was applied to the airborne residual magnetic intensity field data (RMI) to produce Figure 6 showing the NE-SW trending metavolvanics (MV1) magnetic anomaly and numerous distinct magnetic zones. Comparing this Analytic signal map (Figure 6), with the RMI and the RTP colour contour maps, the difference is obvious along the edges of the granitoids, metavolcanics and metasediments contacts, especially at the south-western, eastern, north-eastern, south-eastern and the central parts of the study area. Metasediments, MS1 and MS4 became more definitive while the MS2, MS3 and MS5 were defined to be a single continues body (white polygon in Figure 6). The moderate to low magnetic anomalies of the granitoid intrusives G2, G3, G4, G5 and G6 which are similar to G7, G8 and G9 were mapped better in the analytic signal

map than in RTP and RMI maps; granitoid G6 which reflected signal suggesting it was a secluded intrusive was also defined to be continuous stretching southward. The meta-sediments where also mapped out better in the south-western, central and eastern parts of the area.
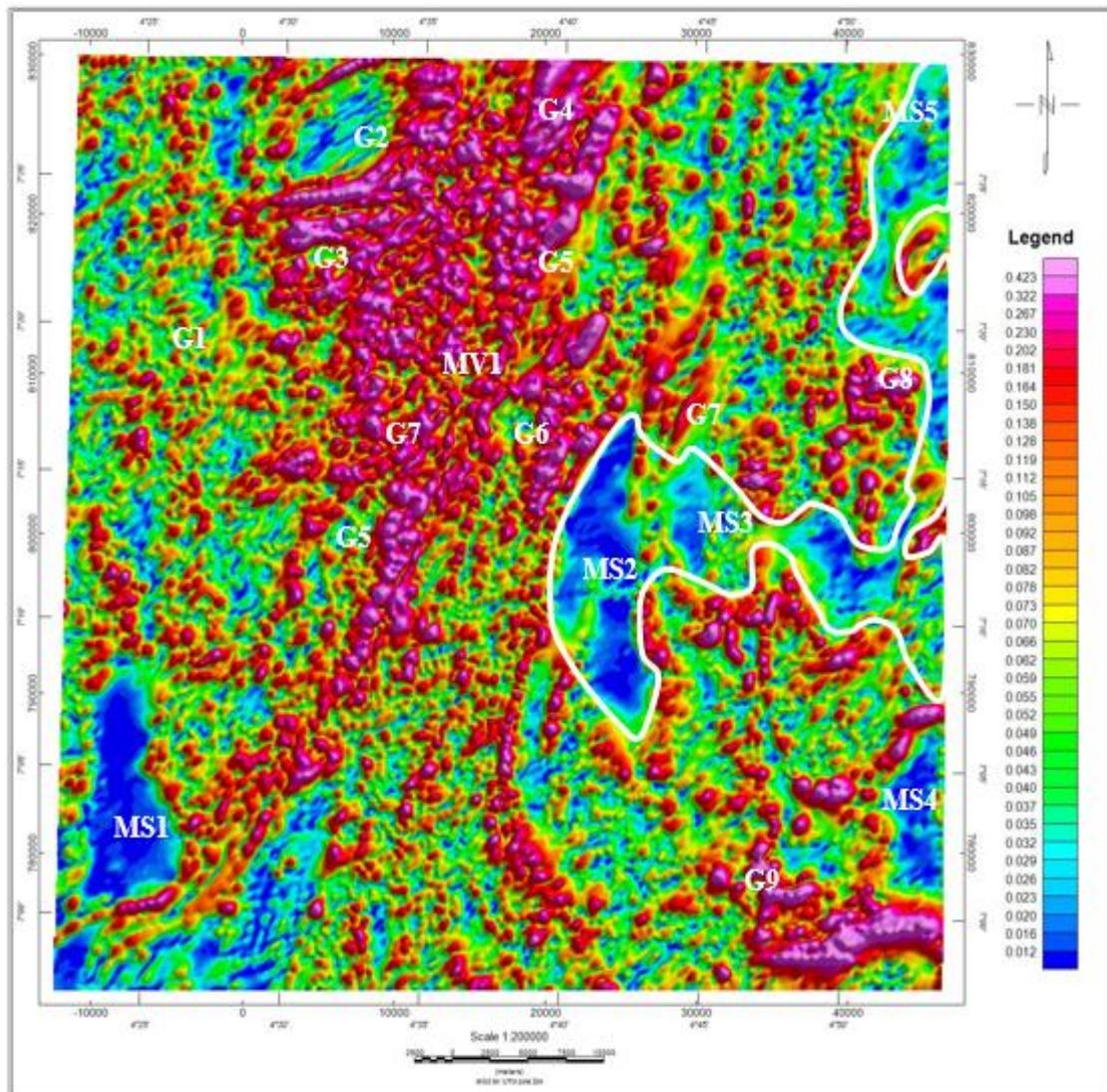

Figure 6: *Analytic Signal Map of the Study Area*

First vertical derivative filter removed long wavelength features of the magnetic field and significantly improved the resolution of closely spaced and superimposed anomalies. Comparison of the first vertical derivative map (Figure 7), with the residual field map (Figure 4), shows an increase in visibility of structural features such as faults (red and black lines), fractures and folds (blue lines).
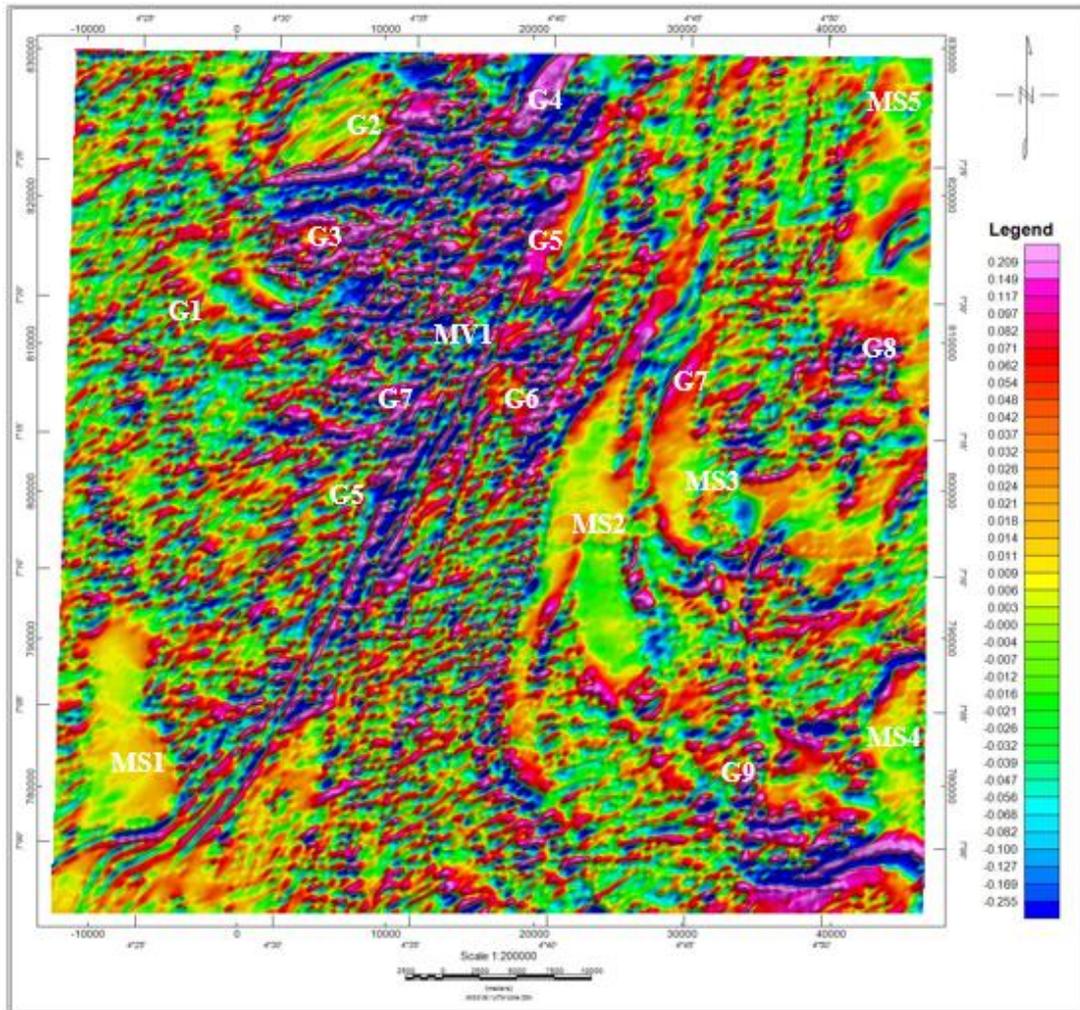
***Figure 7:** First Vertical Derivative Map of the Study Area*

The contact zone between the meta-volcanic (MV) and meta-sediments (MS) interpreted from the FVG shows prominent faulting and shearing. The fault and fracture system trends majorly in the NE-SW direction. This zone is clearly a major fracture system of regional extent and it is likely to have played a fundamental role in gold mineralization. This contact zone is probably an old reactivated structure, as it appears to have guided numerous granitoid intrusions such as G2, G3,G4, G5 and G6 (Figure 4 and Figure 5), which are localized along the contact zone.

The fracture within granitoids most likely acted as the principal conduit for hydrothermal activity of the area in the western, eastern and southern parts of the fault belt. The study area also features crosscutting fault systems trending NNW to N, NE and E-W directions representing the various tectonic episodes associated with the schist belt of western Nigeria. The granitoids within the area have caused severe folding of MV and MS along their boundaries. The intensity of the intrusion is responsible for majority of the faults and shearing occurring along the MV-MS boundary. A large number of faults and folds have been interpreted using filtered airborne magnetic dataset, notably, the analytical signal filter, FVD and TDR (Figure 8). From the maps three deformation events were identified. The early deformation event (D1) is defined to be a ductile deformation producing folds whose axial planes trends NNE-SSW, the second deformation event (D2) resulted in the reactivation of the D1 structures particularly the folds in the NE-SW direction. The third deformation event (D3) produced a transgressive deformation starting with ductile deformation resulting in the development of NE-SW to EW oriented structures observed at the boundary of the metasediment at the central part of the area, brittle deformation occurring at later stages of the D3 event producing fractures oriented in the NE-SW and EW direction which are more associated with the Ife-Ilesha, and reactivated some D1 and D2 faults and fractures.

The area is dominated by a series of NE-SW trending fractures and folds which are interpreted as high angle fault and fold structures formed during regional NW-SE compression resulting in a high degree of shearing and faulting at the contact zone of the meta-sedimentary and metavolcanic hence providing potential accommodation for hydrothermal fluid.
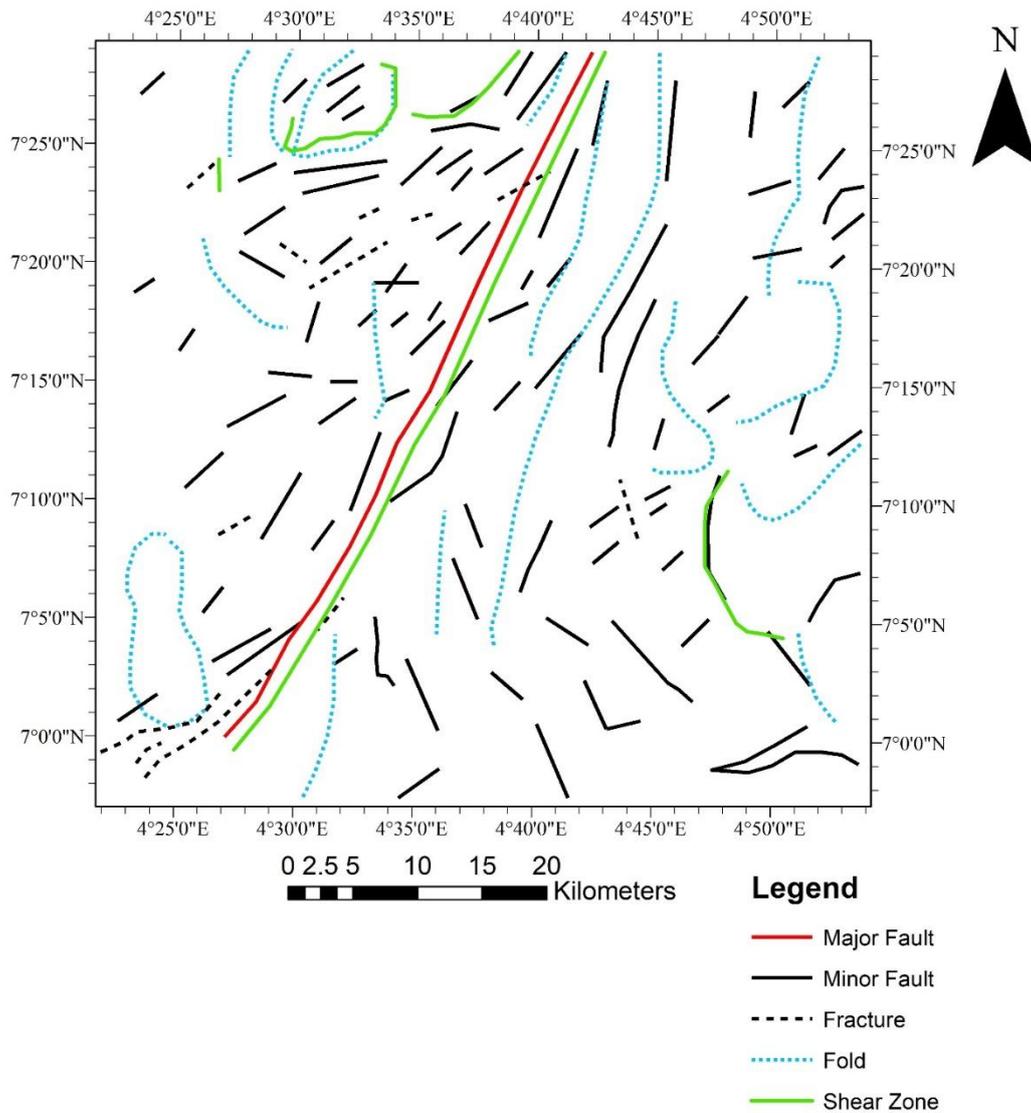
Figure 8: *Interpreted Structural Map of the Study Area*

The intrusive granitoids have caused severe faults within the metavolcanics. The presence of homogenous granitoid bodies have resulted in a deviation in the shear movement along the contact zone, and this deviation has created a zone of dilation, which became the focus of hydrothermal activity. The movement of hydrothermal fluids to low pressured zones within the fault zones generated heat which destroyed the magnetic mineral within the host rocks, thus the magnetic anomalies associated with these faults are low. The interpreted geology and structures from the magnetic data was used to develop a model of the area (Figure 9).
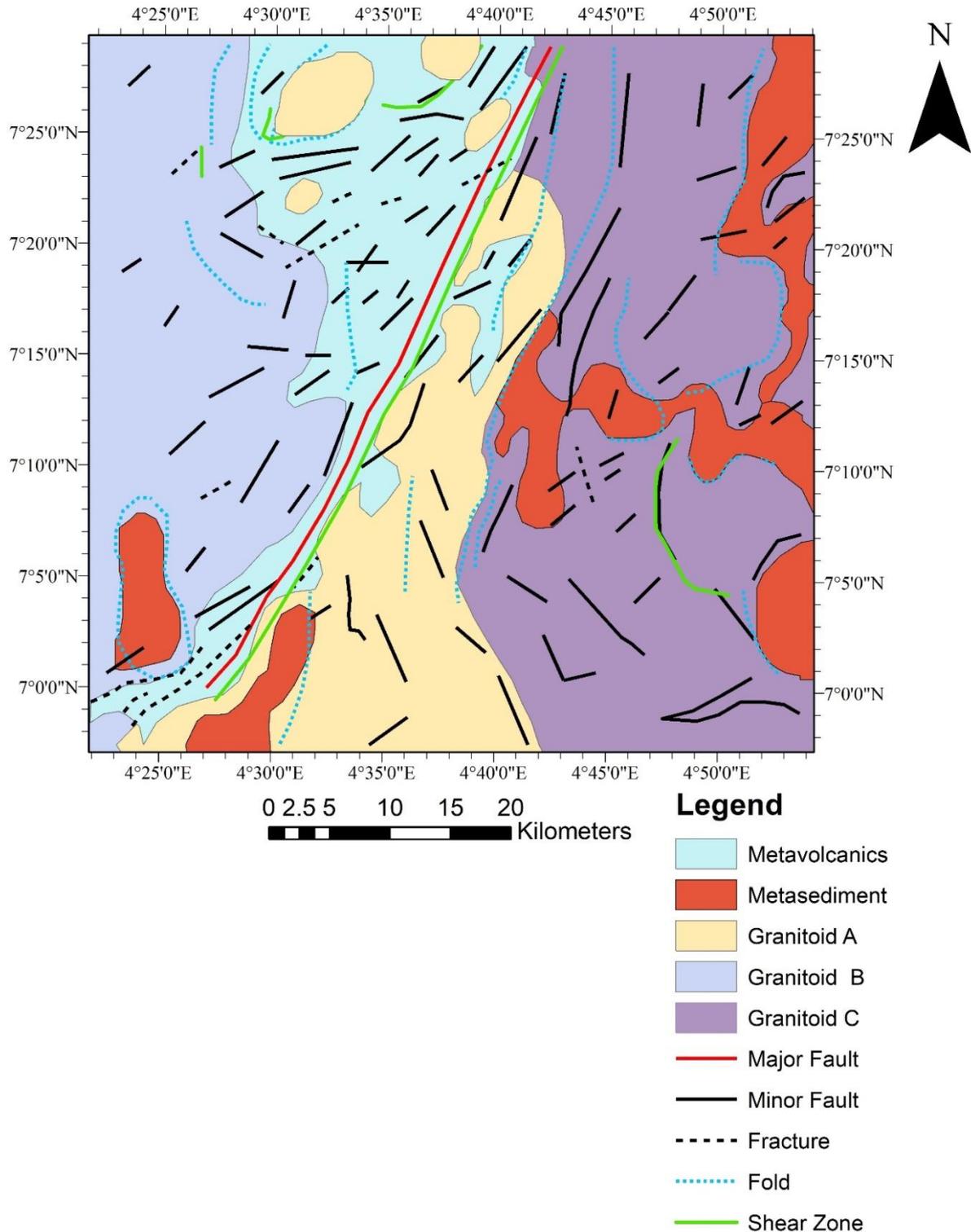
Figure 9: *Proposed Structural and Geological Map Delineated from Aeromagnetic Data*

3.2   Interpretation of Radiometric data
        A number of potassium (K), uranium (U) and thorium (Th) radiometric anomalies are evident in the radiometric survey data. A number of potassium anomalies occur in the radiometric survey image (Figure 10). Strong anomalies occur in the west, central, east and south-east and with granitoid mapped in airborne magnetic interpretation; hence it is defined by high K granitoid (G1) intrusive.
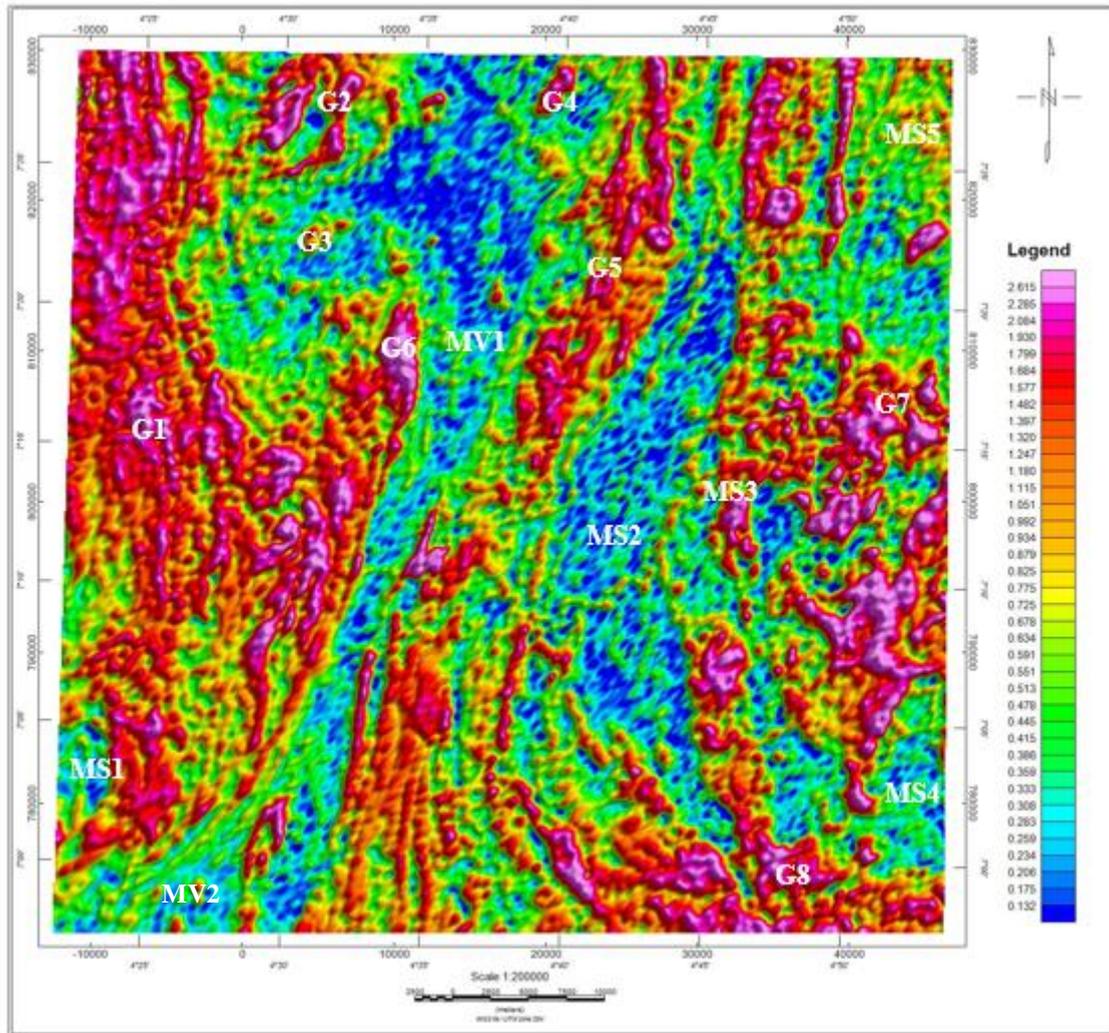
Figure 10: *Potassium Concentration Map in the Study Area*

Potassium radiation essentially comes from K feldspar, predominantly microcline and orthoclase or micas such as muscovite and biotite which are common in felsic igneous rocks (e.g. granite) and are low in mafic rocks (e.g. basalts and andesite) but virtually absent from dunite and peridotites (Manu,1993), hence the weak K signature in the metavolcanic. The metasediments also recorded moderate to low anomalies of immobile and mobile Th and U (Figure 11, Figure 12) respectively, although some high traces of these radioelements can be found within the formation. The Metavolcanic units MV1 show moderate K concentration which corresponds to the schist belt. The metavolcanic MV2 show high signature (Figure 10) which distinctively defines the boundaries with the MV and the granitoids.
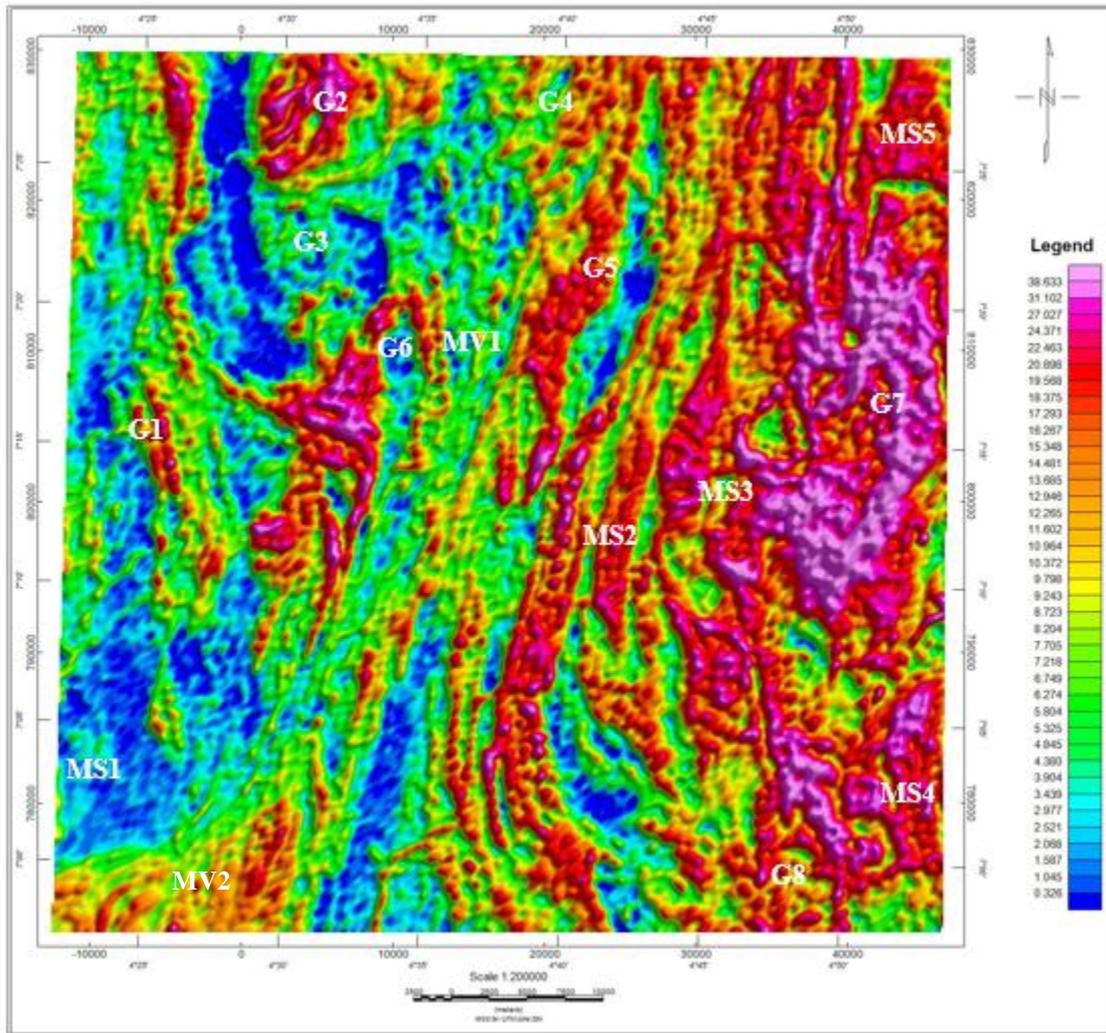
***Figure 11:** Thorium Concentration Map in the Study Area*

High Th concentrations are closely related to felsic minerals and low Th concentrations are related to mafic minerals (Shives *et al.,* 2000). The granitoids at the western and central parts of the area registered moderate to low Th concentration (Figure 11) while those at the eastern corner registered high Th content. The strong thorium concentration at the southern and south-western parts of the study area is as a result of highly weathered colluvial deposits into the lowlands. Thorium is generally considered very immobile (Silva *et al.,* 2003), thus the regions with low thorium concentration suggest Th was mobilized in hydrothermally altered systems. The low Th patterns shows alteration patterns in the different rocks and along lithologic boundaries and within these zones are faults and shears which host hydrothermal fluid which leach Th concentration. Two major granitoids are defined in the area; the first is a high K and weak Th anomalies granitoid, recorded in the western regions which correspond to the belt-type granitoids *i.e.* G1, G3, G4 and G6.
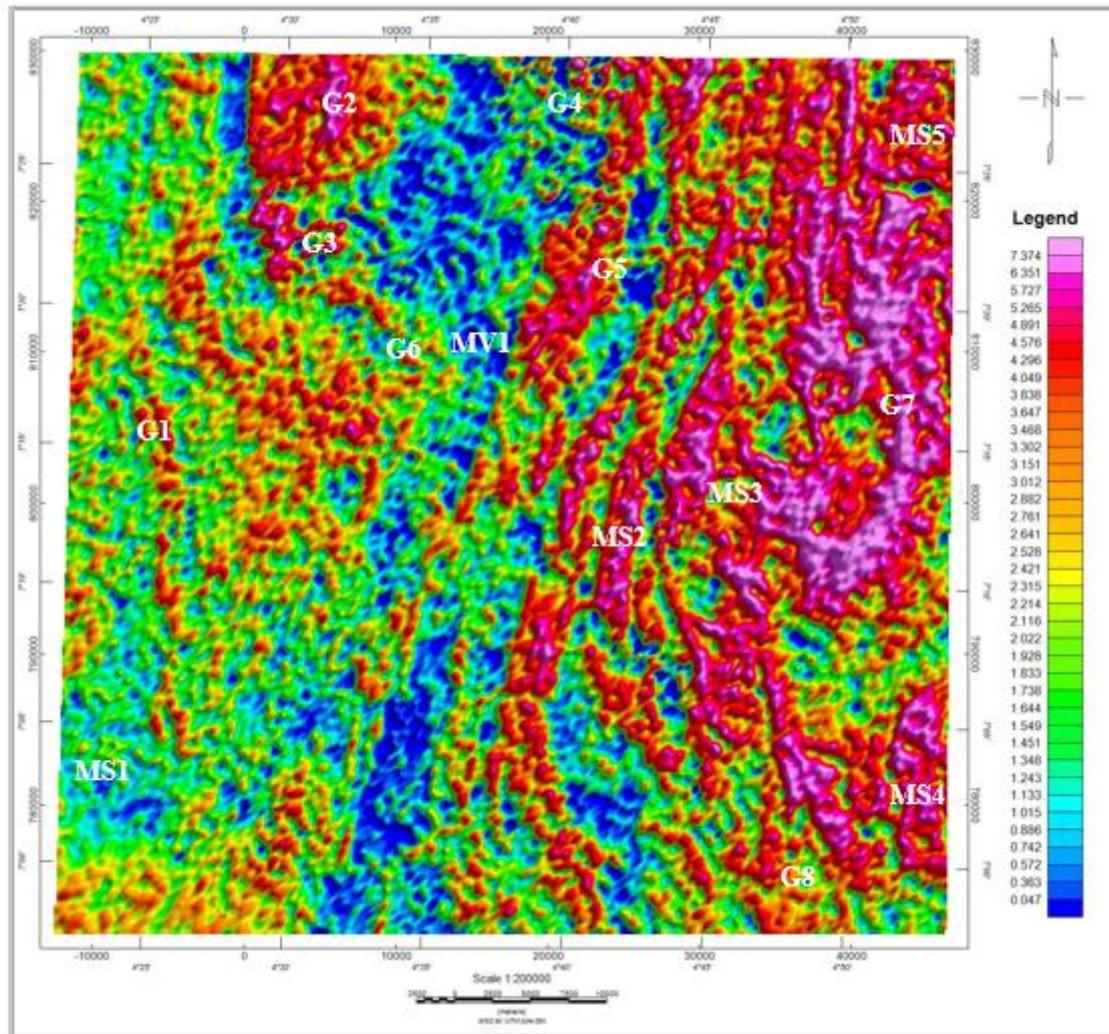
Figure 12: *Uranium Concentration Map in the Study Area*

The eastern and north-eastern and south-eastern parts of the study area are associated with high Th signature (Figure 11) and U signature (Figure 12) with the south-western, western, north-western and central parts recording weak Th and U concentrations.

Thorium-potassium ratio (Th/K) concentrations map (Figure 13) enhances alteration signatures. Mafic volcanic rocks generally lack K-bearing minerals and K enrichments accompany hydrothermal alteration processes but are not accompanied by Th (Dickson and Scott, 1997), therefore increase in K content and decrease in Th/K ratio observed for the metavolcanic rocks (MV) is indicative of hydrothermal alterations. K and other metal constituents are added to the host rock by hydrothermal solutions, and it is easily observed in mafic units or along lithologic contacts where hydrothermal alteration such as silicification is intensive.
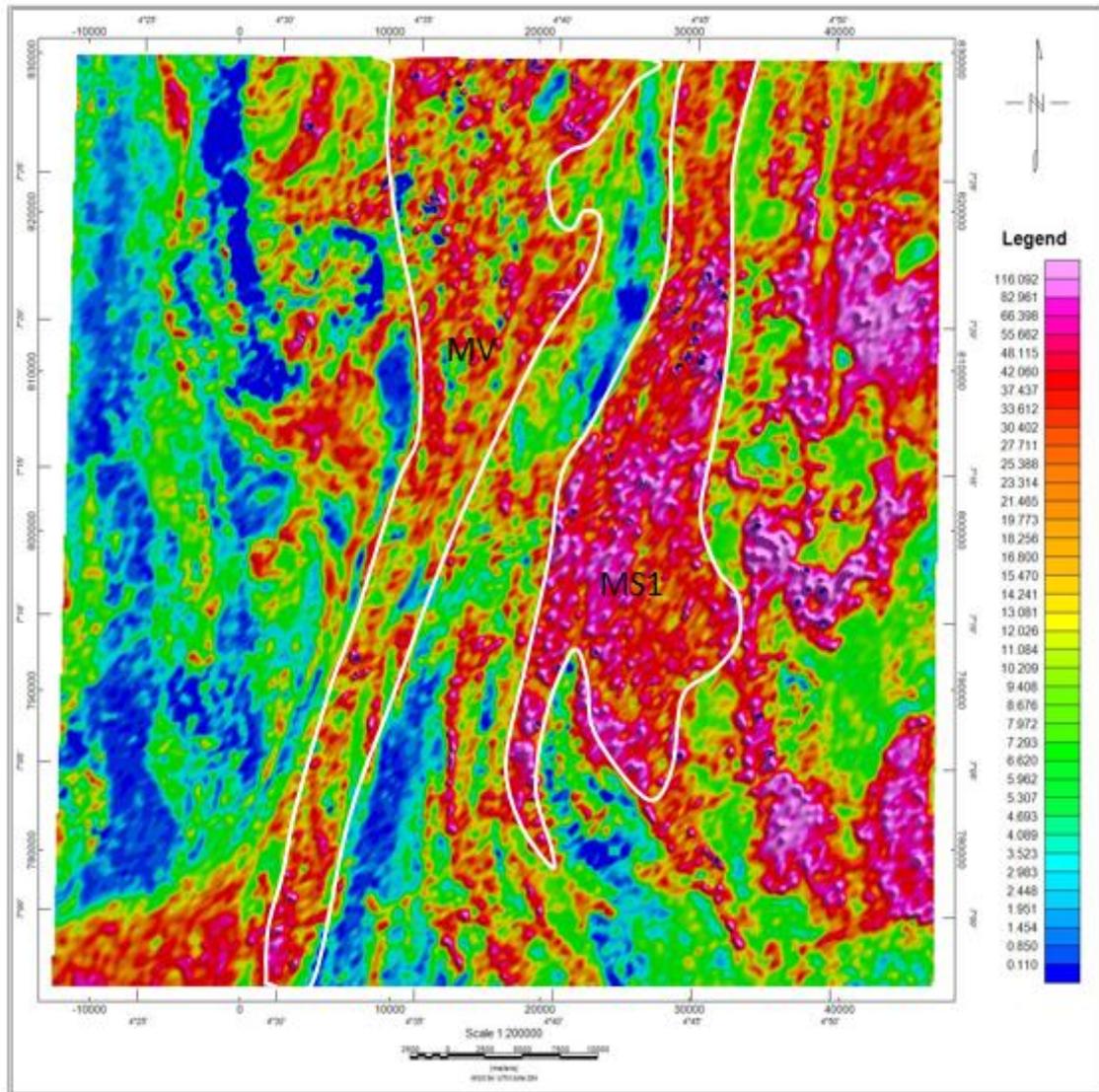
***Figure 13:** Thorium Potassium ratio Map in the Study Area*

Increase in K and decrease in Th occurrences are noted along the faulted north to southwest meta-volcanic and central meta-sediments contact zones (white polygon in Figure 13) and are interpreted as favourable alteration environment for variety of ore deposits. Some possible gold mineralization zones show increases in K and Th such as the central metasediments (MS1 in Figure 13); this suggests that Th was mobilized in hydrothermally altered systems in that zone.

The Ternary map (Figure 14) comprises colours generated from the relative intensities of the three components and represents subtle variations in the ratios of the three bands.
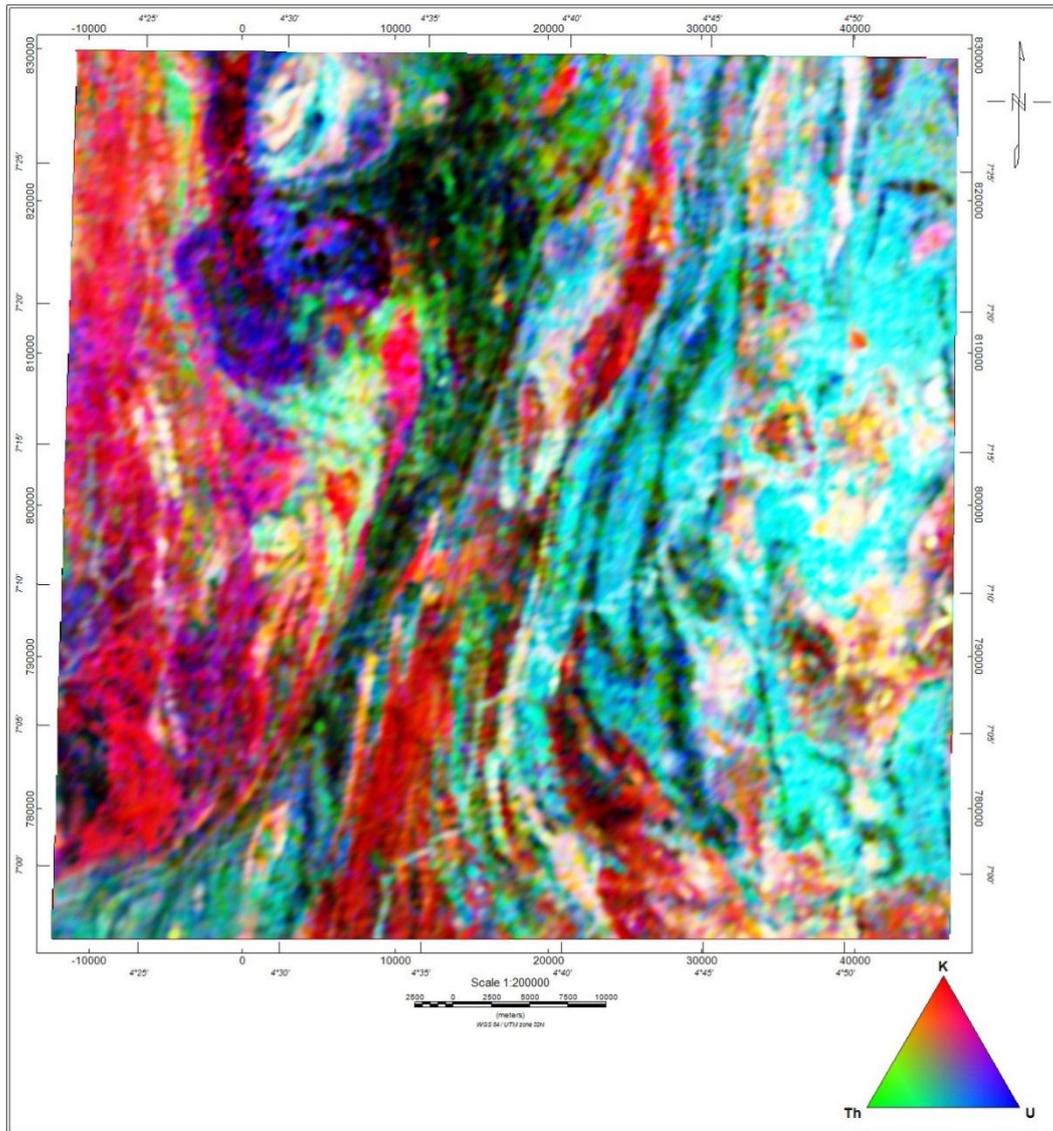
***Figure 14**: Radiometric Ternary Map in the Study Area*

Potassium was assigned to red, thorium to green and uranium to blue. The white areas in the ternary map indicate high concentration of K, Th and U resulting from felsic volcanic materials. The magenta shows areas of high K and U but low Th concentrations while the yellow indicates areas of high K and Th but low U concentrations. The ternary map shows high Th concentration in the schist at the north stretching to the south-west of the area. The granitoid at the western part of the area shows high K concentration with abundance in all three elements. The strong U anomaly associated with the belt-type granitoids, G2, G3, G4, G5 and G6 suggests that these granitoids may be younger than G1 granitoid due to long denudation period of weathering which might have depleted most of the U concentration of G1. The previously defined granitoid at the eastern part of the area was better define and show abundance in all the three elements and significant high concentration of K and U respectively and is interpreted to be gneiss granite. The extent of the metavolcanic defined at the north and stretches to south-west direction of the study area, is also defined with high K concentration and some traces of U are given a magenta colour; this strong correlation is based on the fact that the meta-sediments are made up of the potash-rich regolith which come in the form of muscovite, biotite, aplite and pegmatite. The metavolcanic is interpreted as part of the Ife-Ilesha Schist belt. The intrusive granitoid within the schist belt that outcrops at the highland is clearly defined in the Ternary image. The metasediment rich in Th and U are interpreted to be peltic schist at the eastern part of the area.

The radioelement ternary image (Figure 14) was used to outline the major lithological units which describe different radioactivity levels. The defined lithologic unit was used to develop the geologic map of the study area (Figure 15).
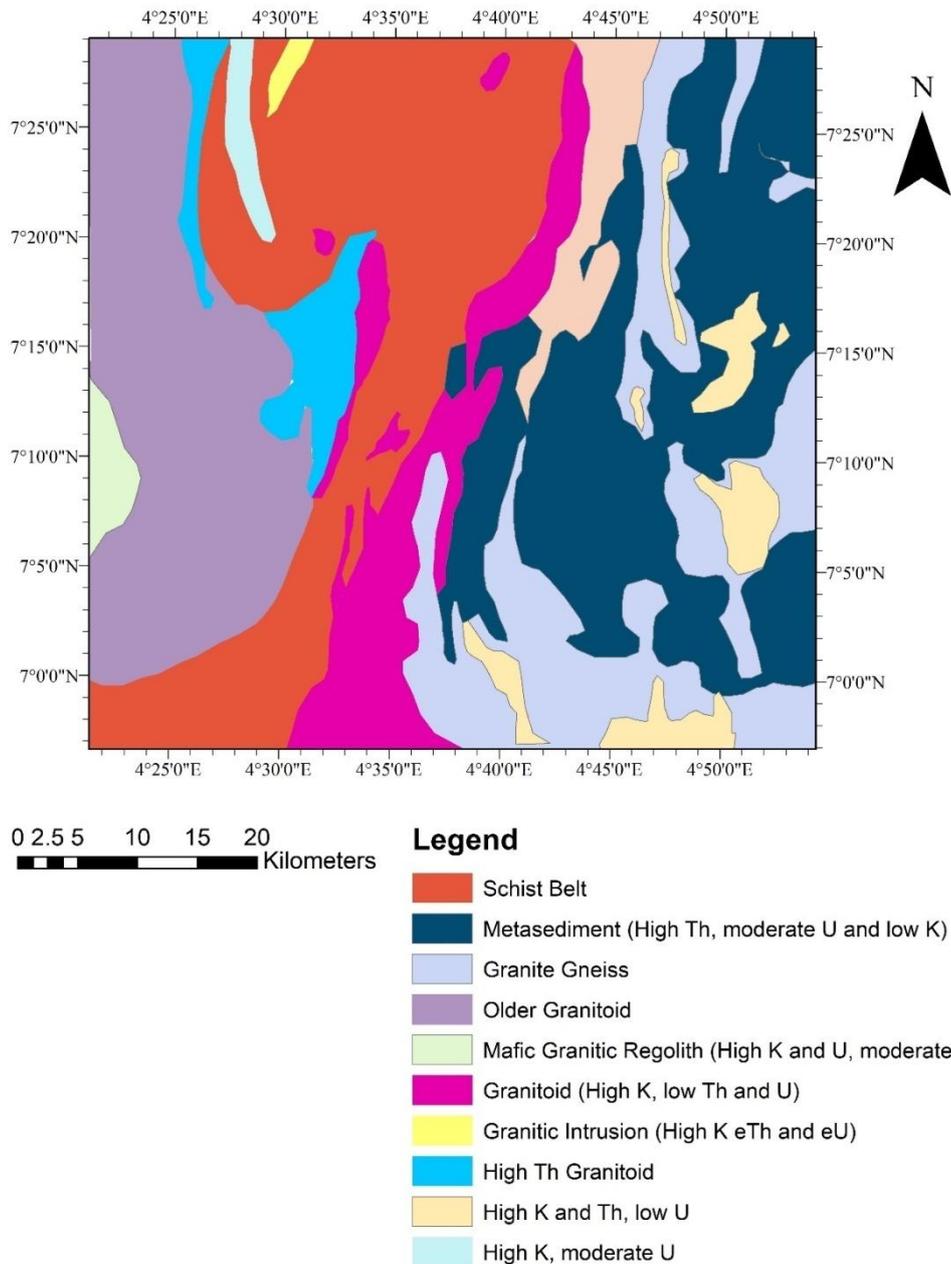
Figure 15: *Proposed Geological Map Delineated from Airborne Radiometric Data*

The interpreted airborne magnetic and radiometric data was integrated to develop a structural and geologic model of the area (Figure 16). Low Th concentration, mobilization of immobile Th concentration and K concentration within the metavolcanic (schist belt) and metasediment (pelitic schist) define hydrothermally altered zones along lithologic boundaries. The altered regions A1, A2, A3 and A4 in Figure 16 which is associated with the schist belt has high potassium and high uranium element. It also shows low magnetic anomalies due to the increase in rock permeability (intense faulting and shearing thus the ability to host hydrothermal fluids). Graphite, mica, and euhedral to anhedral disseminated Fe sulphides observed in the host rocks in the study area are interpreted to be hydrothermal alteration products, potentially related to gold mineralization. The altered region A5, A6, A7 and A8 (Figure 16) which is associated with the metasediment (schist) at the east of the study area has high potassium and thorium concentration with low magnetic response. Aeromagnetic analysis identified high magnetic contrast between rock bodies along the contact zone, interpreted as a potential pathway for fluid migration and mineralization. The fracture system and the fault cut across NE-SW trending structures (Figure 8), thus rendering these contact zones more permeable and fractured for accumulation of hydrothermal fluids. The NE-SW major structure within the schist belt (S1) is of much importance. It cuts across the contact zone of the geological unit and as well as fractures and fault structures along its path.

To identify possible ore deposits in the study area, both structural and alteration patterns were taken into consideration. High structural connectivity and areas of intensive alterations reflected as low magnetic anomalous and high K concentration were considered particularly, where the two alteration types coincide and also marked by faults, fault intersections, fractures and shear zones.

The altered zone marked A2, A3, A4, A5, A6 and A7 (Figure 16) and structures (folds fractures and faults) S1, S2, S3 and S4 are areas with high potential for gold mineralization with A3, A4, A5, A6 and A7 bearing the most potential. The hydrothermal alteration zone A1 that marked the contact between the metavolcanic and the granitoids are also potential target. An integrated geological map from radiometric and magnetic datasets established links between lithology, structures and hydrothermal alteration patterns. The relationship shows that the hydrothermal system is structurally controlled and majorly limited to any specific lithology or host rock. Moreover, the area is also marked by quartz veins, concordant with the potential mineralized zones allocated along the contact of the metavolcanic and granitoids, indicating the region of higher fluid pressure and accumulation of silicate minerals.
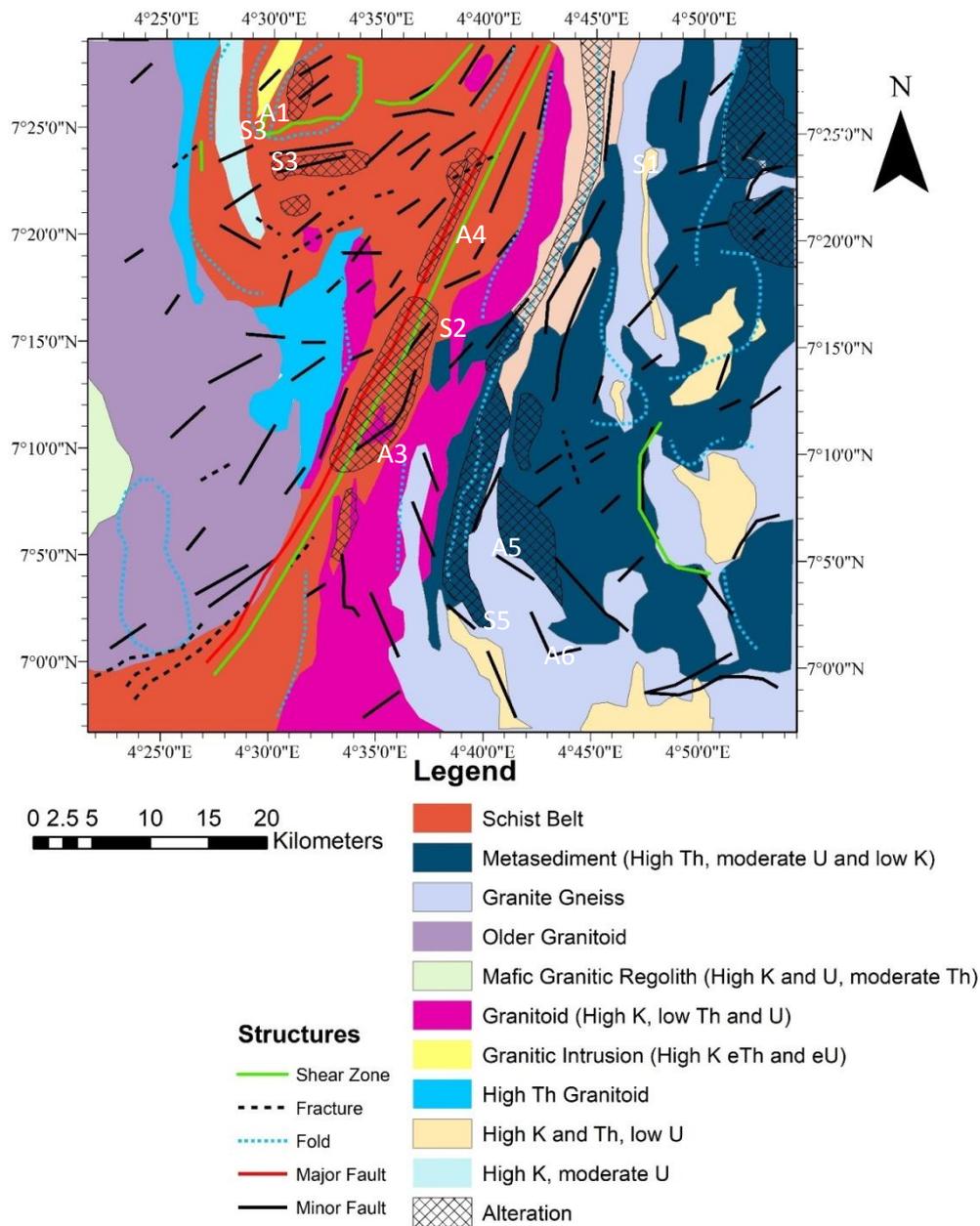

Figure 16: *Proposed Structural Geological Map of the Study Area*

IV. Conclusion

The Ife-Ilesha Schist Belt is a highly faulted, fractured and strain shear belt within the basement complex of southwestern Nigeria which is part of the larger West African Shield. The vertical derivative and tilt derivative maps were used to develop a composite structural map while analytic signal and ternary map were used to build a geologic model of the study area. The area is dominated by a series of high angle faults, NE-SW trending fractures and folds structure which resulted from a regional NW-SE compression which gave rise to a high degree of shearing and faulting at the contact zone of the meta-sedimentary and metavolcanic, hence providing potential accommodation for hydrothermal fluid. The area is characterized by hydrothermally altered zones at the north, north-east and center of the study area and these altered zones fall within and at the contact between metavolcanics and metasediments within the study area. The altered zones are closely related to the interpreted geologic structures. The mapped geological structures, lithology and hydrothermally altered zones which play the role of mineralization indicators defined from the aeromagnetic and radiometric datasets have added to the proposal of many authors such as Hubbard (1960), Rahaman (1976), Kayode (2006) and Adelusi *et al*. (2013) regarding the area as potential host of commercial gold deposits.

Reference

[1]. Annor, A. E. (1995). U-Pb zircon Age for Kabba-Okene Granodiorite Gneiss: Implication for Nigeria's Basement Chronology. African Geoscience Review 2, pp. 101-105

[2]. Ansari, A. H. and Alamdar, K. (2011). A New Edge Detection Method Based On The Analytic Signal Of Tilt Angle (ASTA) For Magnetic And Gravity Anomalies. Iranian Journal of Science & Technology A2, Pp. 81 – 88

[3]. Armstrong, M. and Rodeghiero, A. (2006). Airborne Geophysical Techniques in Aziz. Coal Operators' Conference (pp. 113-131). University of Wollongong and the Australasian Institute Mining and Metallurgy.

[4]. Dada, S. S., Lancelot, J. R. and Briqueu L (1989) Age and origin of the annular charnockitic complex at Toro, Northern Nigeria: U-Pb and Rb-Sr evidence. Journal of African Earth Sciences 9 2 227-234.

[5]. Dada, S. S. and Respaut, J. P. (1989). La monzonite a fayalite de Bauchi bauchite): Nouveau emoin d'ún magmatisme syntectonique pan-africain au nord du Nigeria. Compte Rendus Academie des Sciences de Paris 309 (II) 887-892.

[6]. Dada, S.S., Briqueu, L. Harms, U., Lancelot, J.R. and Matheis, G. (1995) Charnockitic and monzonitic Pan-African series from north central Nigeria: Trace-element and Nd, Sr, Pb isotope constraints on their petrogenesis. Chemical Geology (Isotope Geoscience) 124 233-252.

[7]. Dickson, B. L. and Scott, K. M. (1997). Interpretation of aerial gamma ray surveys-adding the geochemical factors. AGSO Journal of Australian Geology and Geophysics, 17 (2):187- 200.

[8]. Grant, N. K. (1970). Geochemistry of Precambrain basement rocks from Ibadan, southwestern Nigeria. Earth & Planetary Science Letters 10 29-38.

[9]. Hubbard, F. H. (1960). Geological mapping of southern Nigeria. Bull. Geol. Surv. Niger. No. 38

[10]. Kayode, J.S., (2006) Ground Magnetic Study of Jeda-Iloko Area, Southwestern Nigeria and Its Geologic Implications. M. Tech. Thesis Federal University of Technology, Akure, Nigeria.

[11]. Luo, Y., Wang, M., Luo, F. and Tian, S. (2011). Direct Analytic Signal Interpretation Of Potential Field Data Using 2-D Hilbert Transform. Chinese Journal of Geophysics Vol.54, No.4, 2011, Pp. 551 - 559

[12]. Manu, J. (1993). Gold Deposits of Birimian Greenstone Belt in Ghana: Hydrothermal Alteration and Thermodynamics.PhD Thesis, Braunschweiger Geologisch-Paläontologische Dissertationen, Vol. 17,Braunschweig.

[13]. Miller, H. G. and Singh, V. (1994). Potential field tilt — A new concept for location of potential field sources: Journal of Applied Geophysics, 32, no. 2–3, 213–217, doi: 10.1016/0926- 9851(94)90022 - 1.

[14]. Murphy, B. S. (2007). Airborne geophysics and the Indian scenario. J. Ind. Geophysics Union, 11 (1), 1-28.

[15]. Nabighian, M. N. (1972). The analytical signal of two-dimensional magnetic bodies with polygonal cross- section: its properties and use for automated anomaly interpretation Geophysics, 37(3):507– 517.

[16]. Neves, P. S., Bruguier, O., Vauchez, A., Bosch, D., Rangel, J. S. and Mariano, G. (2006). Timing of crust formation, deposition of supracrustal sequences, and Transamazonian and Brasiliano metamorphism in the East Pernambuco belt (Borborema Province, NE Brazil): Implications for western Gondwana Assembly. Precambrian Research 149 197-216.

[17]. Olusegun, O., Kehinde-Phillips and F.T. Gerd, (1995) The Mineralogy and Geochemistry of the Weathering Profiles Over Amphibolite, Anthophillite and Talc-Schists in Ilesa Schist Belt, Southwestern Nigeria, Journal of Mining and Geology, 31 (1): 53 – 62.

[18]. Ondo State Ministry of Economic Planning & Budget. (2010). Ondo State. A publication of the Ondo State Ministry of Economic Planning & Budget, Ondo, Nigeria.

[19]. Ondo State Ministry of Lands, Housing & Environment. (2000). Ondo State. A publication of the Ondo State Ministry of Economic Planning & Budget, Ondo, Nigeria.

[20]. Rahaman, M. A. and Emofurieta, W. O. (1983). The potassic granites of Igbeti area: Further evidence of the polycyclic evolution of the Pan-African Belt in Southwestern Nigeria. Precambrian Research 22 75-92.

[21]. Rahaman, M. A. and Lancelot, J. R. (1984). Continental crust evolution in SW Nigeria: Constraints from U/Pb dating of pre-Pan-African gneisses. In: Rapport dáctivité 1980-1984. Document Travaux Centre Geologie et Geophysique, Montpellier, II 4 41.

[22]. Rahaman, M. A., Tubosun, I. A. and Lancelot, J. R. (1991). U-Pb geochonology of potassic syenites from southwestern Nigeria and the timing of deformational events during the Pan-African orogeny. Journal of African Earth Sciences 13 387-395.

[23]. Rahaman, M.A., (1976) A review of the Basement Geology of Southwestern Nigeria. Kogbe, C.A. (ed.), Geology of Nigeria, Elizabeth Publishing Co., pp 41 – 58.

[24]. Shives, R., Charbonneau, B. and Ford, K. (2000). The detection of potassic alteration by gamma-ray spectrometry-recognition of alteration related to mineralization. Geophysics-Wisconsin the Tulsa-Society of Exploration Geophysicists, 65(6): pp. 2001–2011.

[25]. Silva, A. M., Pires, A. C., McCafferty, A., Moraes, R. and Xia, H. (2003). Application of airborne geophysical data to mineral exploration in the uneven exposed terrains of the Rio Das Velhas greenstone belt. Revista Brasileira de Geociências, 33(2):17-28.

[26]. Telford, W. M., Geldart, L.P. and Sheriff, R. E. (1990). Applied Geophysics (2nd Edition ed.).Cambridge University Press.

[27]. Tubosun, I. A., Lancelot, J. R., Rahaman, M. A. and Ocan, O. (1984). U-Pb Panafrican ages of twocharnockite-granite association from southwestern Nigerian. Contributions to Mineralogy and Petrology 88 188-195.

[28].   Van Schmus, W. R. and Brito, B. B. (2003). The Serido Group of NE Brazil, a late Neoproterozoic pre-to syn-collisional basin in West Gondwana: insights from SHRIMP U-Pb detrital zircon ages and Sm-Nd crustal residence (TDM) ages. Precambrian Research 127 287-327

[29].   Verduzco, B., Fairhead, J. D., Green, C. M. and Mackenzie, C. (2004). New insights into magnetic derivatives for structural mapping: The Leading Edge, 23, 116–119, doi: 10.1190/1.1651454.

[30].   Wilford, J. R., Bierwirth, P. N. and Craig, M. A. (1997). Application of airbornegamma-ray spectrometry in soil/regolith mapping and applied geomorphology. AGSO J. Austr. Geol. Geophys.; 17(2):201216.